Observed response of stratospheric and mesospheric composition to sudden stratospheric warmings.

M. H. Denton[1,2], R. Kivi[3], T. Ulich[4], C. J. Rodger[5], M. A. Clilverd[6], J. S. Denton[7], and M. Lester[8].

1. Center for Space Plasma Physics, Space Science Institute, CO 80301, USA.
2. New Mexico Consortium, Los Alamos, NM 87544, USA.
3. Space and Earth Observation Centre, Finnish Meteorological Institute, Sodankylä, Finland.
4. Sodankylä Geophysical Observatory, Sodankylä, Finland.
5. Department of Physics, University of Otago, Dunedin, New Zealand.
6. British Antarctic Survey (NERC), Cambridge, UK.
7. Nuclear and Radiochemistry (C-NR), Los Alamos National Laboratory, Los Alamos, USA.
8. Department of Physics and Astronomy, University of Leicester, Leicester, UK.

ABSTRACT: In this study we investigate and quantify the statistical changes that occur in the stratosphere and mesosphere during 37 sudden stratospheric warming (SSW) events from 1989 to 2016. We consider changes in the in-situ ozonesonde observations of the stratosphere from four sites in the northern hemisphere (Ny-Ålesund, Sodankylä, Lerwick, and Boulder). These data are supported by Aura/MLS satellite observations of the ozone volumetric mixing ratio above each site, and also ground-based total-column O_3 and NO_2, and mesospheric wind measurements, measured at the Sodankylä site. Due to the long-time periods under consideration (weeks/months) we evaluate the observations explicitly in relation to the annual mean of each data set. Following the onset of SSWs we observe an increase in temperature above the mean (for sites usually within the polar vortex) that persists for >~40 days. During this time the stratospheric and mesospheric ozone (volume mixing ratio and partial pressure) increases by ~20% as observed by both ozonesonde and satellite instrumentation. Ground-based observations from Sodankylä demonstrate the total column NO_2 does not change significantly during SSWs, remaining close to the annual mean. The zonal wind direction in the mesosphere at Sodankylä shows a clear reversal close to SSW onset. Our results have broad implications for understanding the statistical variability of atmospheric changes occurring due to SSWs and provides quantification of such changes for comparison with modelling studies.

1. Introduction

The phenomenon of a Sudden Stratospheric Warming (SSW) was first identified by *Scherhag* [1952] using radiosonde observations of the stratospheric temperature above Berlin. Scherhag clearly demonstrated that the temperature of (usually cold) stratospheric air underwent an extremely rapid increase (~50°C) in January and February of 1952. Such "*explosive warmings in the stratosphere*" were originally termed the "*Berlin Phenomenon*" [*Scherhag*, 1952]. In subsequent studies the broad physical and chemical mechanisms that underpin SSWs were revealed (e.g. *Perry* [1967], *Matsuno* [1971], *Trenberth* [1973], *Schoeberl* [1978]; *Dütsch and Braun* [1980], *Schoeberl and Hartmann* [1991]). In brief, planetary-scale waves from the troposphere carry momentum and energy upwards into the stratosphere and mesosphere. The breaking of these waves in the upper-stratosphere/mesosphere can cause the disruption and/or break-up of the polar vortex (PV) [*Matsuno*, 1971]. The PV usually carries colder air from the mesosphere down into the stratosphere during the polar winter. Odd-nitrogen species (NO_x) from the mesosphere are also transported downward from the mesosphere in the PV. NO_x-species are long-lived during darkness and chemical reactions with NO_x constitute the major loss mechanism for stratospheric ozone (O_3) during the polar winter [*Brasseur and Solomon*, 1986]. Details of the chemical and dynamical variation of ozone in the Arctic wintertime have since been outlined in detail (see *Tegtmeier et al.* [2008a] and references therein). In contrast, the main source of O_3 is the Brewer-Dobson circulation [*Dobson et al.*, 1929; *Brewer*, 1949; *Dobson* 1956] (see also *Solomon* [1999] and *Butchart* [2014] and references therein). The planetary wave-breaking that accompanies the onset of a SSW transports heat from lower latitudes and accelerates the Brewer-Dobson circulation [*McIntyre*, 1982]. This leads to a rapid warming of the stratosphere from its previous low-temperature state. Additionally the downwards transport of NO_x is also terminated, leading to a cessation of O_3 losses through chemical reactions with NO_x, while the primary source of O_3 is largely unchanged. In combination, these processes usually lead to a rapid increase in O_3 levels in

63 the upper stratosphere and mesosphere immediately following a SSW, with the altitudinal
64 dependence of O_3 behaviour during SSWs strongly dependent on altitude (cf. *de la Cámara et al.*
65 [2018a]).
66
67 Although SSWs have been observed in both northern and southern latitudes, they are
68 predominantly a northern hemisphere phenomenon since planetary waves in the southern
69 hemisphere usually have a much lower wave-amplitude. The literature contains a large number of
70 recent studies where the various effects of SSWs in the stratosphere and mesosphere have been
71 investigated, both observationally and theoretically (e.g. *Sofieva et al.* [2012], *Scheiben et al.*
72 [2012], *Kuttippurath and Kikulin* [2012], *Päivärinta et al.* [2013], *Damiani et al.* [2014]; *Shepherd*
73 *et al.* [2014], *Lukianova et al.* [2015], *Manney et al.* [2015], *Strahan et al.* [2016], *Meraner and*
74 *Schmidt* [2016], *Butler et al.* [2015; 2017], *Solomonov et al.* [2017]; *de la Cámara et al.* [2018a;
75 2018b]; *Smith-Johnsen et al.* [2018]). The main processes occurring in the atmosphere before and
76 after SSWs have been determined extensively in the literature and are summarized graphically in
77 Figure 1.
78
79 SSWs have received increasing attention within the community in recent years. This is
80 predominantly due to the connections between SSWs, tropospheric weather, and surface climate in
81 the northern hemisphere (e.g. *Kretschmer, et al.* [2018], and references therein). Determining the
82 occurrence date of a SSW allows forecasters to predict likely weather patterns much further in
83 advance [*Tripathi et al.*, 2015; *Pedatella et al.*, 2018]. Additionally, since the effects of SSWs
84 propagate upwards in altitude, as well as downwards, determining their morphology assists in
85 understanding topics as diverse as electron densities in the ionosphere (e.g. *Chau et al.* [2012]) and
86 satellite drag (e.g. *Yamazaki et al.* [2015]). As with many other dynamic terrestrial phenomena, the
87 classification of SSWs has proven somewhat difficult to formalize with different definitions of the

88 various types of SSW having been identified in the literature. The recent works of *Butler et al.*
89 [2015] and *Palmeiro et al.* [2015] assess the various criteria being used to identify and classify
90 SSWs and provide the impetus for more-rigid definitions throughout the community.
91
92 Despite the large number of studies of individual SSWs in the literature, there have been few
93 investigations that quantify the statistical variability in composition that occur before during, and
94 after these events (cf. *Strahan et al.* [2016]). Each event is certainly different, with different initial
95 conditions in the atmosphere, different driving mechanisms, and differing durations. Modelling
96 studies are used increasingly to provide predictions of changes in the atmosphere during SSWs, and
97 to subsequently derive the physical and chemical basis for these changes. However, such models
98 require observational data for comparison. The over-arching aim of the current study is to quantify
99 the changes that occur in the stratosphere and mesosphere regions of the atmosphere during SSWs,
100 in a statistical manner, and hence reveal the variability of atmospheric effects caused by these
101 events. Previous analyses have generally considered the effects of single SSWs during a particular
102 year. Such studies usually consider the time-series of the parameter under consideration (e.g. how
103 O_3 at a particular location changes in time). However, the observed changes during such events
104 (which may last days, weeks, or even months), are usually provided in addition to the natural
105 variation of the parameter (that would be expected to take place whether a SSW occurred or not).
106 In contrast to such analyses, the work in this study is intended to reveal (and quantify) the statistical
107 changes that occur, on average during SSWs, with respect to the underlying (naturally occurring)
108 annual variation (see also *Päivärinta et al.* [2013]; *Ageyeva et al.* [2017]). Such *seasonal-*
109 *corrections* to the data (to ascertain the deviation from the natural variation) were previously made
110 with respect to changes in O_3 during solar-proton events (SPEs) [cf. *Denton et al.*, 2017; 2018] and
111 the same techniques are used in the current study.
112

The data and analysis techniques used in this study are summarized in Section 2. Results are presented in Section 3 and discussed in detail in Section 4. A summary of the main findings and the conclusions to be drawn from this study are to be found in Section 5.

2. Data and Analysis

The study of *Bulter et al.* [2015] correctly points out that the definitions of SSWs have changed over time and that a single definition to fit all users would likely be impossible. They also wisely notes: "…*history suggests that a true standard definition of SSWs is at best ambiguous and at worst nonexistent*". The problem with standards is that there are so many of them. The analyses undertaken in this study concern 37 SSWs occurring between 1989 and 2016. These events are a combination of the previously published events identified in Table 2 of *Butler et al.* [2017] and Table 4.1 in *Ehrmann* [2012] with the events after 2013 taken from the recent literature. Here we follow *Butler et al.* [2017] with SSWs defined as when the daily-mean zonal-mean zonal winds at 10 hPa and 60° N first change from westerly to easterly between November and March. The winds must return to westerly for twenty days between events.. Table 1 contains the onset timing of the events used (further details of the events can be found in *Butler et al.* [2017] and *Ehrmann* [2012]). A caveat to statistical analysis of SSWs is that in each year there may be a single warming, or multiple warmings (denoted in the literature as "*first warming*", "*major warming*", "*final warming*", etc.). The durations, and indeed the actual definitions, of each of these (e.g. "*displacement events*", "*split events*") is highly variable throughout the literature (see *Butler et al.* [2015] and *Palmeiro et al.* [2015] for a detailed discussion of SSW definitions). The atmosphere will clearly be in a somewhat different and unique state for the first warming, compared to the final warming, with each event having a different time-history. However, there are certainly similarities between all events particularly since the onset of a SSW occurs due to the break-up/disruption of the PV, driven by breaking of planetary waves. It is these similarities that are investigated here. Separating out

the statistical effects of multiple warmings during a single year is not possible due to the limited number of events and is beyond the scope of the current study. The main goal in the current study is to quantify the mean changes taking place in stratospheric and mesospheric O_3 during a typical SSW (with other parameters also being investigated). We do not aim to investigate the differences between individual events but rather concentrate on the mean perturbations to be expected during an "average" SSW onset. Since each event is different the most appropriate methodology to use is superposed-epoch analysis (sometimes known as composite analysis). This analysis is based on ordering the data from each event based on an "epoch time", here identified as the time of SSW onset (from Table 1). The mean variation of each parameter with relation to the epoch time can then be determined (along with percentiles, standard-deviation, etc.). This methodology was previously used in the studies of ozone changes during SPEs [*Denton et al.*, 2017; 2018] as well as other phenomena relating to particle precipitation into the atmosphere and subsequent changes in atmospheric chemistry (e.g. *Kavanagh et al.* [2012], *Denton and Borovsky* [2012], *Blum et al.* [2015]).

The data sets to be analyzed via superposed-epoch analysis relate to the abundance of O_3 in the stratosphere and mesosphere. In addition, we also examine other selected parameters that are known to affect the production, loss, and transport of ozone in the atmosphere. These include the variations in stratospheric and mesospheric NO_2 (due to its link to the loss of O_3), the speed and direction of the prevailing atmospheric winds (due to its role in the transport of O_3), and the temperature (due to linkages with both the source and the loss processes connected with O_3). The data sets associated with these variables are described in Sections 2.1-2.4 below.

2.1 ECC ozonesonde data

Frequent high-resolution ozonesonde observations are made at dozens of sites around the globe.

Many utilize balloon-borne Electrochemical Concentration Cell (ECC) detectors to provide the ozonesonde partial pressure and temperature as a function of pressure (and geopotential altitude) from the ground up to ~38 km altitude [*Deshler et al.*, 2008; 2017, *Kivi et al.*, 2007, *Smit and ASOPOS Panel*, 2014]. The wind direction and speed can also be sampled and recorded. Here, data from ECC ozonesondes launched from four sites are utilized: Ny-Ålesund on the Svalbard archipelago (NY-ÅL); Sodankylä in northern Finland (SOD); (C) Lerwick on the UK Shetland Isles (LER); (D) Boulder in the continental USA (BOU). The observations provide the ozone partial pressure (in mPa), and temperature above each location. The sites are chosen to provide observations that are typically within the PV (NY-ÅL and SOD), close to the edge of the PV (LER), or always outside the PV (BOU). The BOU site is to be used as a 'control' since SSW effects are not generally expected to occur at such low latitudes. The geographic location of the sites, and the average percentage of time that each spends within the PV from January to April are shown in graphical format in Figure 2. Data from these four sites was previously used to determine the role of the PV in the reduction of ozone observed following SPEs [*Denton et al.*, 2017; 2018].

2.2 Aura/MLS satellite data

The Aura satellite was launched in 2004 and carries a Microwave Limb Sounder (MLS) instrument that is designed to measure the temperature and abundance of a wide range of the upper stratospheric and mesospheric constituents, including O_3. A previous MLS instrument with very similar characteristics was flown on the Upper Atmosphere Research Satellite [*Waters et al.*, 1999]. Verification methodology for the instrument can be found in the works of *Jiang et al.* [2007] and *Livesey et al.* [2008]. Here, we use the vertical profile O_3 volume-mixing-ratio data (combined with geopotential height data) above site-specific ground stations (L2, V04) to determine any observed trends and to quantify the morphology of ozone before, during, and after SSW events. These data have already been used in numerous studies of O_3 behaviour in the stratosphere and

mesosphere (e.g. *Manney et al.* [2006], *Boyd et al.* [2007], *Jackson and Orsolini* [2008], *Strahan et al.* [2013], *Damiani et al.* [2014], *Kishgore et al.* [2016]).

2.3 SAOZ ground-based UV-visible spectrometer data

The Network for the Detection of Atmospheric Composition Change (NDACC) operated (Système d'Analyse par Observation Zénithale) SAOZ instrument [*Pommereau and Goutail*, 1988] is situated at Sodankylä and co-located with the SOD ozonesonde launch site. The instrument is a UV-visible spectrometer that provides morning and evening vertical column integrals of the abundance of NO_2 and O_3 that have been used in numerous observational campaigns [*Vaughan et al.*, 1997; *Vandaele et al.*, 2005; *Pommereau et al.*, 2013]. Here, the SAOZ data are used to provide: (a) an independent comparison dataset against which to test the O_3 observations from ozonesondes and Aura/MLS, and (b) to determine any change in total column NO_2 from before, during, and after SSWs (cf. *Ageyeva et al.* [2017]).

2.4 SLICE meteor radar data

A SkiYMET meteor radar known as the Sodankylä-Leicester Ionospheric Coupling Experiment (SLICE) was installed in northern Finland in 2008, positioned at the same location as the SOD ozonesonde launching site discussed above. The instrument transmits at ~36.9 MHz and subsequently measures the Doppler shift of returning echoes from meteors in the upper atmosphere. The meridional and zonal wind speeds in the altitude region from ~80-100 km (upper mesosphere - lower thermosphere) may then be derived from these observations [*Hocking et al.*, 2001]. In previous work *Lukianova et al.* [2015] used the SLICE radar observations during three SSWs to demonstrate that mesospheric cooling occurs prior to stratospheric warming, and that the cooling and warming were of similar magnitudes (~50 K). Here, we utilize the SLICE data to quantify the change in zonal wind direction in the mesosphere that occurs during our set of SSWs (2008-2016).

3. Results

3.1 Ozonesonde results

Data from the ground-based ozonesondes introduced in Section 2.1 are not launched daily at any site (Table 2 and Figure 2). Thus, none of the sites has continuous daily coverage during the 37 SSW-events considered here. Rather than investigate individual events, we carry out a superposed epoch analysis (i.e. composite analysis) of the events to reveal the statistical characteristics of SSWs. The mean O_3 volumetric mixing ratio at each site is first calculated (measurements are usually recorded as O_3 partial pressure) and then plotted as a function of altitude and month and shown in the left column of Figure 3. There is a clear latitudinal trend to the data with the lowest latitude site (BOU) showing the highest mixing ratio and the highest latitude site (NY-ÅL) having the lowest mixing ratio. Strong annual variations at each site are also evident with the highest level of O_3 generally found in northern hemisphere spring and the lowest level occurring in autumn. The peak O_3 mixing ratio occurs at around 30 km altitude for all sites. The mixing ratio plots presented here may be compared directly with the mean ozone partial pressures previously calculated at each site and plotted in Figure 2 of *Denton et al.* [2018] (see also *Kivi et al.*, 2007). The main point to note is that the peak partial pressure of O_3 occurs at ~20 km altitude (the peak of the stratospheric ozone layer) while the peak in the volumetric mixing ratio occurs roughly 10 km higher.

Also shown in the right column of Figure 3 are superpositions of the O_3 mixing ratio at each of the four sites, with respect to the 37 SSWs (these are initially uncorrected for season). Certain trends can immediately be drawn from these plots. Firstly, there is a clear latitudinal variation. The most poleward site (NY-ÅL) shows clear evidence for a sharp increase in the O_3 mixing ratio following the onset of SSWs. The data at SOD and LER show similar trends, although with a less clear

demarcation from before-SSWs to after-SSWs. There is little evidence of a clear systematic variation in the data from BOU during the period under study. However, since the data plotted here are not seasonally-detrended the apparent observed changes cannot be simply attributed to SSWs. The SSWs generally occur at the start of the year when the underlying annual trend at all sites is for an increase in the O_3 mixing ratio. It is essential that this "natural" increase is removed when the underlying aim is to reveal perturbations to the annual trend that are due solely to SSWs.

To correct for seasonal biases in the data, and to quantify the variation in O_3 due solely to SSWs, we again calculate the difference-from-mean at each site. Figure 4 contains these difference-from-mean plots with respect to the temperature (top row), the O_3 mixing ratio (middle row) and the O_3 partial pressure (bottom row). The difference-from-mean of each parameter is plotted with increases (above mean value) shown in shades of red and decreases (below mean value) shown in shades of blue. Values close to the mean value are coloured white. Note: for the temperature, changes from the mean are plotted in °C. For the O_3 mixing ratio and O_3 partial pressure, the changes are plotted as a percentage increase (red) or decrease (blue) from the mean value.

With reference to the temperature, the changes that occur due to SSWs can be found in the top-row of panels of Figure 4. These show numerous interesting features. At NY-ÅL (first column) there is a clear increase in the measured atmospheric temperature over a wide altitude range that commences close to the arrival of SSWs. The maximum difference-from-mean is ~10°C (Figure 4, top left plot) while the absolute change in temperature from a few days before the SSW occurrence to a few days after is ~20 °C (although again there are wide variations in these values on an event-by-event basis). The temperature changes at SOD and LER are similar (although the increase is slightly less than that observed at NY-ÅL) At all three sites the temperature first increases at higher altitudes >30 km a few days before zero epoch. Higher temperatures are subsequently

detected at ~20 km altitude a few days later. Temperature changes persist for up to 40 days (NY-ÅL) although these changes are somewhat altitude-dependent as expected. In contrast with the more poleward locations, there are no systematic changes in temperature evident at the BOU site, which is outside the PV at all times.

With reference to the O_3 mixing ratio during SSWs, the plots in the middle row of Figure 4 also show clear trends. At NY-ÅL, the O_3 mixing ratio shows a clear rapid increase of ~15-20% commencing around zero epoch at altitudes ~20-30 km. This persists for in excess of 30 days (albeit in an altitude-dependent way). The data from SOD and LER are less clear, although the mixing ratio increases to ~10% above of the mean value after zero epoch. Again, there are no systematic changes in mixing ratio evident at BOU.

With reference to the O_3 partial pressure, the plots in the bottom row of Figure 4 show similar features as observed for the mixing ratio. The data from NY-ÅL shows an increase of up to 30% occurring at the same time as the SSW in the altitude region between ~20-30 km. This feature persists for ~30-40 days. A similar magnitude increase is also observed centred on ~10 km altitude, with altitudes around 15-20 km showing a less substantial increase. Again, SOD and LER show some evidence of similar trends (~10% increase) but with much more variation. There are no systematic trends in the O_3 partial pressure in the BOU data.

3.2 Aura/MLS ozone results

Data from the Aura/MLS instrument span the period from Aug 2004-2017 and thus include 15 of the 37 events. However, although the altitudinal resolution is somewhat coarse (compared with the ozonesondes) these data have the advantage of much higher temporal coverage for all of the four selected locations, with daily files usually available. The Aura/MLS data shown in Figure 5

provide independent confirmation of the ozonesonde results (shown in Figure 3 and Figure 4) in the altitudinal region of overlap, and have the added benefit of coverage in altitude up into the mesosphere. Here, data are plotted from 0-80 km altitude although data at altitudes below ~215 hPa (~10 km altitude) should be generally disregarded [*Jiang et al.*, 2007; *Livesey et al.*, 2008].

As with the ozonesonde data, we initially calculate the mean annual variation in the O_3 mixing ratio above each of the four sites and plot this with the same scale as previously used. The results of this are shown in Figure 5. In the altitude region of overlap there are similar trends in the mean annual variations of the Aura/MLS data as were observed by ozonesonde (cf. Figure 3). Notably, the highest mixing ratio is found at the lowest latitude (BOU). The overall magnitude of the averages are similar at all sites, in the altitude region of overlap. The general agreement found between Aura/MLS and ECC ozonesondes provides further confidence in the comparison of MLS data with ozonesonde data during SSWs, despite the MLS dataset only covering years from 2004 onwards (and thus only 15 SSWs).

Figure 5 contains plots of the superposed O_3 mixing ratio observed by Aura/MLS data during 15 SSWs that occurred after Aug 2004. The left column in this figure shows the superposed data uncorrected for season while the right column shows the same data seasonally-detrended (i.e. plotted as a percentage difference-from-mean). For clarity, the difference-from-mean plots are limited in altitude from the stratosphere above 20 km and the mesosphere below 60 km where data reliability, coverage, and altitudinal resolution, are all greatest.

As with the ozonesonde data, it is clear that the O_3 mixing ratio undergoes a sharp and substantial increase with the onset of SSWs, particularly at the highest latitude sites (NY-ÅL and SOD). The mean mixing ratio is increased by ~20% at all altitudes between 20-60 km and persists upwards of

313 40 days. At LER there is some evidence of an increase in the mixing ratio following the SSWs.
314 There is no evidence of an increase in the mixing ratio at BOU. The magnitudes of the changes
315 observed by Aura/MLS (at the sites where an increase is observed) are of a similar order to that
316 seen with the ozonesondes.
317
318 **3.3 NO_2 and O_3 column integrals from SAOZ results**
319 Data from the SAOZ UV-visible spectrometer provide NO_2 and O_3 column abundances at SOD,
320 with which to further confirm the ozonesonde and MLS results for O_3, and also with which to
321 examine the effect of SSWs on total NO_2. As with other parameters, we commence by calculating
322 the mean of the parameter (measured density during both the morning and evening observations) as
323 a function of month. These are plotted in Figure 7. Both NO_2 (left column) and O_3 (right column)
324 show large annual variations during morning (top row) and evening (bottom row) which make it
325 necessary to carry out a seasonally-corrected difference-from-mean analysis to reveal changes in
326 these parameters solely due to SSWs.
327
328 Figure 8 contains plots of the superposed NO_2 and O_3 morning and evening observations as a
329 function of time relative to 36 of the 37 SSWs when data are available. The left column shows the
330 data uncorrected for season and the right column shows the superpositions seasonally-corrected as a
331 difference-from-mean value. The thick black line is the mean of the superposition while the red,
332 blue and purple lines denote the upper quartile, median, and lower quartile of the averages. In these
333 plots there is an apparent slow increase in NO_2 that commences around zero epoch. A sharper
334 increase is also evident for O_3 (both morning and evening). However, the seasonally-corrected
335 plots shown in the right column indicate the true variations linked to SSWs rather than due to the
336 background seasonal variations. The superposed NO_2 profiles for morning and evenings (top two
337 rows) are flat, indicating that the total column-integrated NO_2 at SOD is unchanged by the onset of

a SSW (a result in agreement with the findings of *Sofieva et al.* [2012]). In contrast, the total column O_3 at SOD is actually *decreasing* prior to the SSWs. Following zero epoch there is a rapid increase in total-column O_3 and elevated levels of ozone persist for in excess of 40 days. Note: We also examined the column integral data from the Ozone Monitoring Instrument (OMI) on the Aura satellite with the NO_2 and O_3 column data from SAOZ. The Aura/OMI data do show some evidence of a similar increase in column ozone around the onset of SSWs (not shown) but data from OMI at the high latitude sites are sparse due to the orbit of the satellite and thus have not been considered further.

3.4 Mesospheric winds from SLICE results

The break up of the PV is generally accompanied by a sudden reversal in mean zonal wind direction in the stratosphere and mesosphere. In order to confirm that this reversal occurs for our collection of SSWs we perform a similar analysis as for the other data sets using data from the SLICE meteor radar. Hence we can quantify the change in zonal wind speed at the very top of the mesosphere and close to the mesopause, at the SOD site between 82 and 100 km altitude (data above 100 km altitude were unavailable during these intervals). Figure 9 shows a superposition of the zonal wind speed as a function of time from the onset of SSW for 9 of the 37 SSW events after 2008 when data are available. This figure shows wind with a west-to-east direction as having a positive zonal wind speed (red) and an east-to-west direction as having a negative zonal wind speed (blue). Despite the limited SSW dataset, a robust trend is evident. Strong positive wind speeds (west-to-east) occur until a few days prior to zero epoch. West-to-east winds at SOD are indicative of the anti-clockwise PV winds over the northern pole during winter (cf. Figure 1 of *Denton et al.*, 2018]) The zonal wind direction ceases to be strongly westwards-to-eastwards a few days prior to zero epoch and then changes sharply to an east-to-west direction suddenly, very close to zero epoch, confirming the disruption/break-up of the PV over SOD around this time. This sharp trend

363 is (on average) short-lived, lasting only ~4 days. After zero epoch the wind direction is much more
364 variable with both easterly and westerly winds being observed, although this is somewhat
365 dependent upon altitude.
366
367 ## 4. Discussion
368 Very complex (temperature-dependent) chemistry and transport governs the abundance of O_3 in the
369 stratosphere/mesosphere [e.g. *Brasseur and Solomon*, 1986; *Newman et al.*, 2001; *Tegtmeier et al.*,
370 2008a]. Elucidating how the O_3 abundance changes provides clues as to the most important of
371 these processes before, during, and after SSWs. The results of the current study, documented
372 above, provide quantification of the statistical changes typically occurring in various physical
373 parameters during SSWs, with reference to the mean state of the stratosphere and mesosphere.
374
375 For the 37 SSWs studied here the in-situ balloon ozonesonde observations at four sites demonstrate
376 an increase in the mean temperature at the highest latitude site (NY-ÅL) of ~10°C at stratospheric
377 altitudes of ~15-30 km (Figure 4, top left panel). Lower-latitude sites (SOD and LER) show a
378 similar, although less strong, increase as might be expected - these sites are not always within the
379 PV during the winter months (see Table 2). The volume mixing ratio at NY-ÅL increases by ~20%
380 above the mean at the onset of the SSWs with a slightly lower increase observed at SOD and LER.
381 No increase in temperature, O_3 mixing ratio, or O_3 partial pressure are observed at the control-site
382 of BOU, which is consistently outside the PV.
383
384 The mean upper stratospheric/mesospheric O_3 mixing ratios, as measured by Aura/MLS, are shown
385 in Figure 5. The absolute change and the difference-from-mean changes in these satellite-measured
386 parameters during SSWs are shown in Figure 6. The increase in O_3 mixing ratio at NY-ÅL and
387 SOD (~20% in the altitude region 20-60 km) following the SSWs agrees very well with the

388 ozonesonde observations, in the overlapping altitude region. As noted above, the larger altitude
389 range provided by the satellite observations also provides additional insights into the altitude range
390 of the SSW-linked changes.
391
392 The average annual variation of total-column NO_2 and O_3 at Sodankylä are shown in Figure 7. The
393 difference-from-mean of these constituents (Figure 8) clearly shows that the total-column NO_2 is
394 completely unchanged by SSWs while total-column O_3 undergoes a sharp increase. Of course, our
395 results do not provide any information regarding the *altitudinal distribution* of NO_2 during SSWs.
396 It is perfectly possible (and perhaps likely) that the altitudinal distribution of NO_2 will change
397 during SSWs. However, investigation into changes in the composition during SSWs were
398 previously carried out for the stratosphere, mesosphere, and lower thermosphere by *Sofieva et al.*
399 [2012]. The authors used GOMOS data to show that enhancements in NO_3 were strongly
400 (positively) correlated with the temperature changes that followed SSWs (during 2003-2008),
401 although there were no clear changes noted in NO_2 [*Sofieva et al.*, 2012] - in agreement with
402 findings in the current study.
403
404 The decrease in total-column O_3 before SSWs, also shown in Figure 8, is indicative of the usual
405 polar-night chemical loss (dominated by NO_x and O_3 chemistry) due to the presence of a PV. Once
406 such losses cease, at the onset of the SSW, then O_3 increases rapidly (since the main loss
407 mechanism is absent while the transport of ozone continues - cf. Figure 1). Finally, the meteor
408 radar observations at SOD confirm the clear reversal in mesospheric zonal wind direction that
409 occurs at the onset of the SSWs used in this study (Figure 10 - cf. *Lukianova et al.*, 2015).
410
411 In the context of previously published work, the results presented in this study have provided
412 observational statistical quantification of the increases of upper stratospheric and mesospheric

ozone following SSWs. For the major SSW in 2009, *Tao et al.* [2015] conclude that after the event, poleward transport increased with this particular SSW accelerating the polar descent and tropical ascent of the Brewer–Dobson circulation, and thus leading to the rapid increase in stratospheric O_3. The importance of this "resupply" of ozone into the polar stratosphere was also highlighted by *Manney et al.* [2011] following the exceptional loss of Arctic ozone in 2011.

The work of *de la Cámara et al.* [2018a] provides particularly robust analysis of the changes expected during SSWs based on results from the Whole Atmosphere Community Climate Model (WACCM) version 4. In that study the authors discuss the change in O_3 in terms of the continuity equation of ozone concentration in WACCM and attribute the observed O_3 increase as being due to the temporal offset between ozone eddy transport and diffusive ozone fluxes. Despite the different scales, there are clear similarities between the average O_3 changes occurring following SSWs presented in Figure 6 of this current study and the O_3 changes plotted in Figure 3 in *de la Cámara et al*. [2018a], which add further observational evidence for their conclusions.

Our previous work on stratospheric ozone considered the effects of SPEs on stratospheric ozone during the polar winter, and the role of the PV upon the chemical destruction of O_3 [*Denton et al.*, 2017; 2018]. These statistical studies showed clear statistical losses in stratospheric O_3 following SPEs but the analysis gave no consideration to years with, or without, a SSW. The differing roles of SPEs and SSWs have also been investigated by *Päivärinta et al.* [2013]. They showed that following a SSW, a strong PV reformed and that this PV could lead to enhanced downwards transport of NO_x species. There is also evidence that descent rates at the vortex edge may be much greater than descent rates in the main PV [*Tegtmeier et al.*, 2008b]. SPEs generally create NO_x species at mesospheric (and/or upper stratospheric) altitudes [*Seppälä et al.*, 2008]. These species then descend in the PV and cause chemical destruction of O_3 in the stratosphere/lower-mesosphere.

438 In contrast, and as shown here, SSWs cause a disruption of the PV and subsequent increases in O_3.
439 These two competing effects need to be independently determined and here modelling work is
440 essential. A complicating issue for event studies is the state of the atmosphere prior to an event
441 such as an SSW or SPE. The study of *de la Cámara et al.* [2017] indicated that conditions in the
442 stratosphere prior to a SSW event were important in the evolution/occurrence of the SSW.
443
444 In contrast to examining the geographic distribution of O_3, we are unaware of any definitive study
445 where the vorticity of the atmosphere is treated explicitly in the data analysis. For such a study, the
446 analysis could proceed with the data ordered with respect to *vorticity* rather than *geographic*
447 *position*. For example, H_2O is a good tracer for the PV in the stratosphere/mesosphere, having a
448 low mixing ratio inside the vortex [*Scheiben et al.*, 2012]. Our current and future work is focused
449 on exploring such explicit connections between O_3 and the polar vortex location. While direct
450 concurrent observations of vorticity and O_3 may be sparse, reanalysis datasets (e.g. MERRA2,
451 ERA-Interim/ERA-5, JRA55) can provide a statistical means to better reveal connections between
452 O_3 and the polar vortex.. However, as noted by *Butler et al.* [2015], such reanalysis data sets rely
453 on satellite observations of back-scattered sunlight and during darkness these data sets rely heavily
454 on the underlying model, and thus must be used with full knowledge of their assumptions and
455 limitations. Our future work is also intended to reveal any differences that may occur in the
456 downwards transport of NO_x (and other) species from the main PV and from the edge of the PV.
457
458 Understanding (and accurately modelling) changes in the atmosphere during SSWs remains an
459 important and timely issue [e.g. *Tripathi et al.*, 2015, *Kretschmer, et al.*, 2018, *Pedatella et al.*,
460 2018]. The frequency and strength of SSWs have also been discussed as factors in how
461 anthropogenic and/or long-term climatic changes in the atmosphere are manifested (e.g.
462 *Kuttippurath and Nikulin* [2012]). This current study has quantified the changes that occur in the

463 atmosphere during SSWs, with respect to the underlying annual changes. This is particularly
464 necessary in order to allow direct model-to-data comparison, once seasonal detrending of the data
465 have been carried out.
466

467 5. Conclusions and Summary

468 To conclude, the work carried out in this study has quantified the changes occurring in the O_3
469 mixing ratio, temperature, total-column O_3, total-column NO_2, and mesospheric winds during 37
470 SSWs between 1989 and 2016 (or subsets thereof due to the availability of experimental data)
471 Using the superposed-epoch technique has allowed the changes that occur due to SSWs to be
472 identified with respect to the natural underlying variability.
473

474 The main findings of this study, in relation to the 37 SSWs in this study, are summarized below:
475

476 **1. Locations consistently inside the PV show strong changes linked to the timing of SSWs.**
477 **Changes are less evident for sites occasionally inside the PV, and no changes are observed at**
478 **sites consistently outside the PV.**
479

480 **2. A sudden increase in mean temperature (prior to the SSW) is first observed at ~60 km**
481 **altitude and subsequently at lower altitudes for the two high-latitude sites. The average**
482 **duration of the temperature increase at these sites is ~40 days.**
483

484 **3. An increase in O_3 (of ~20% above the monthly mean) is observed at the two highest**
485 **latitude sites. This persists for ~40 days. There is good agreement between the statistical**
486 **ozonesonde observations and the Aura/MLS observations.**
487

488 **4. The total-column NO_2 is unchanged during SSWs. The total-column O_3 decreases prior to**
489 **zero-epoch and then increases sharply. This increase persists for in excess of 40 days.**
490

491 ## 6. Acknowledgements

492 Ozonesonde data used in this study were retrieved from the World Ozone and Ultraviolet Radiation
493 Data Centre (https://woudc.org/). We thank David Moore, Peter von der Gathen, and Bryan
494 Johnson for provision of the data used here. Aura/MLS data may be retrieved from the NASA Data
495 and Information Services Center (https://daac.gsfc.nasa.gov/) and we thank all members of the
496 MLS team for provision of the data. SAOZ spectrometer data used here are available online
497 (http://saoz.obs.uvsq.fr) and we thank J-P. Pommereau and F. Goutail for their provision. SLICE
498 meteor-radar data are available by contacting Thomas Ulich at SGO (thomas.ulich@sgo.fi).
499

500 MHD is supported by NSF GEM program award number 1502947 and NASA Living With A Star
501 grants NNX16AB83G, NNX16AB75G and 80NSSC17K0682. Research at FMI was supported by
502 the Academy of Finland (grant number 140408); an EU Project GAIA-CLIM; the ESA's Climate
503 Change Initiative programme and the Ozone_cci sub-project in particular. We thank NASA and
504 NSSDC for the Earth images used in Figures 1 and 2,. MHD wishes to thank Niel Malan for wise
505 words and especially thank all at the FMI Arctic Research Centre, the Sodankylä Geophysical
506 Observatory, and the SSC for their hospitality during his visit to Sodankylä in the spring of 2018.
507
508

509

YEAR	MONTH	DAY	DAY OF YEAR
1989	2	21	52
1990	2	12	43
1991	2	4	35
1992	1	13	13
1993	3	7	66
1994	1	3	3
1994	3	29	88
1995	2	3	34
1995	3	22	81
1996	3	29	89
1997	12	24	358
1998	3	28	87
1998	12	14	348
1999	2	24	55
2000	3	19	79
2000	12	20	355
2001	1	2	2
2001	2	10	41
2001	12	27	361
2002	2	16	47
2003	1	17	17
2004	1	3	3
2005	2	1	32
2005	3	11	70
2006	1	20	20
2007	1	2	2
2007	2	22	53
2008	2	21	52
2009	1	23	23
2010	1	26	26
2011	2	1	32
2011	3	25	84
2012	1	17	17
2013	1	17	17
2014	3	31	91
2015	1	5	5
2016	3	16	76

510

511 **TABLE 1**: *Dates of SSWs used in the analysis and taken from Table 2 of Butler et al. [2017] and*

512 *Table 4.1 in Ehrmann [2012].*

513

514

Site	Latitude (GLAT)	Longitude (GLON)	# Ozonesondes in Analysis (Range)	Polar Vortex (PV) in Winter ?	Reference
Ny-Ålesund	**78.90**	**12.00**	**2350** (1991-2016)	**Usually within PV (>70% of time)**	***Rex et al. [2000]***
Sodankylä	**67.37**	**26.63**	**1886** (1989-2016)	**Usually within PV (>50% of time)**	***Kivi et al. [2007]***
Lerwick	**60.15**	**-1.15**	**1289** (1994-2016)	**Occasionally within PV (~15% of time)**	***Smedley et al. [2012]***
Boulder	**40.01**	**-105.27**	**1287** (1991-2016)	**Never Within PV (0% of time)**	***Johnson et al. [2002]***

TABLE 2: *Location of sites used in this analysis with the corresponding range of data available at each site.*

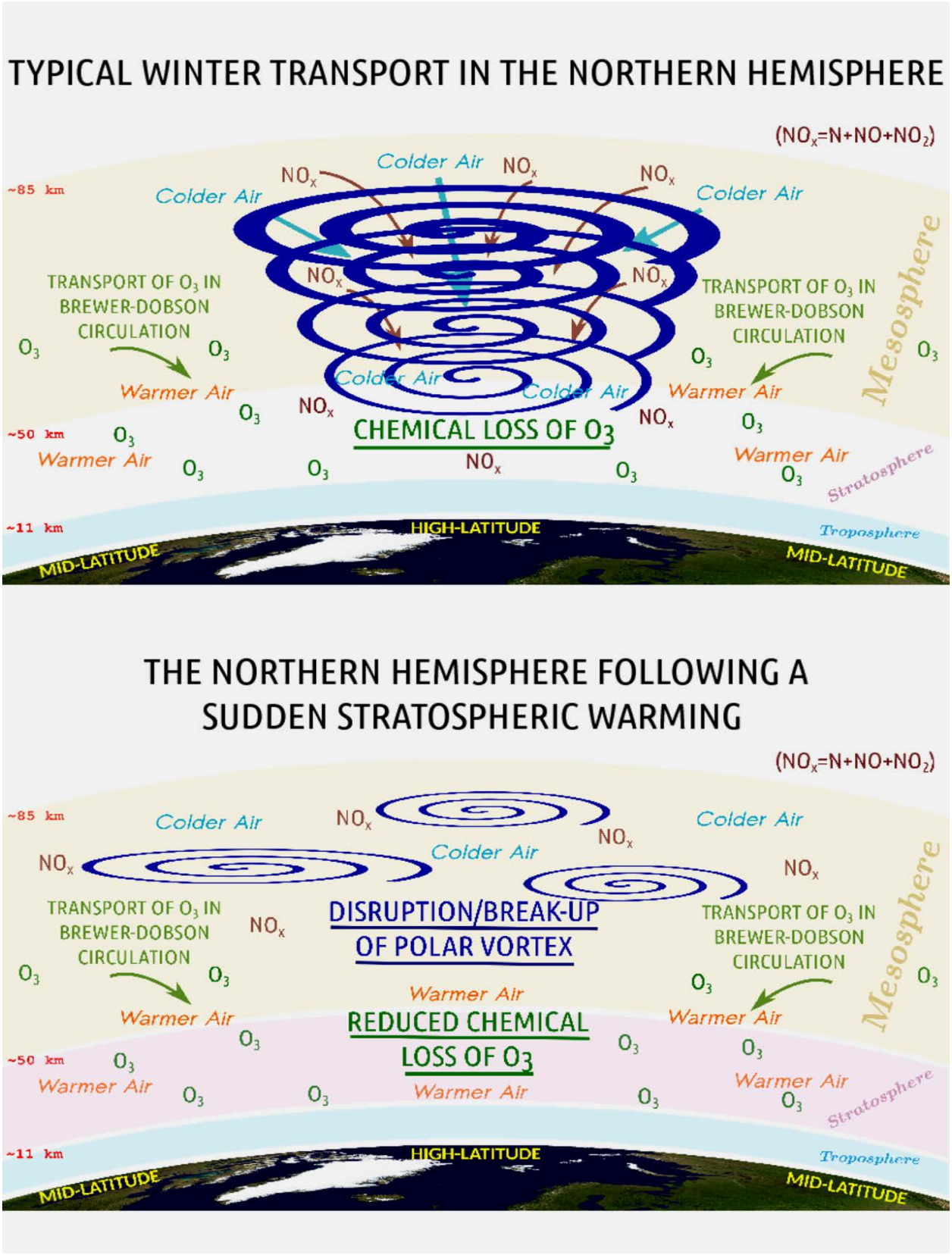

Figure 1. *Atmospheric processes in the northern hemisphere (top) and some of the changes that occur during SSWs (bottom). The strength of the polar vortex (dark-blue/purple) is closely linked to the amount of ozone in the stratosphere/mesosphere (Figure created via Inikscape).*

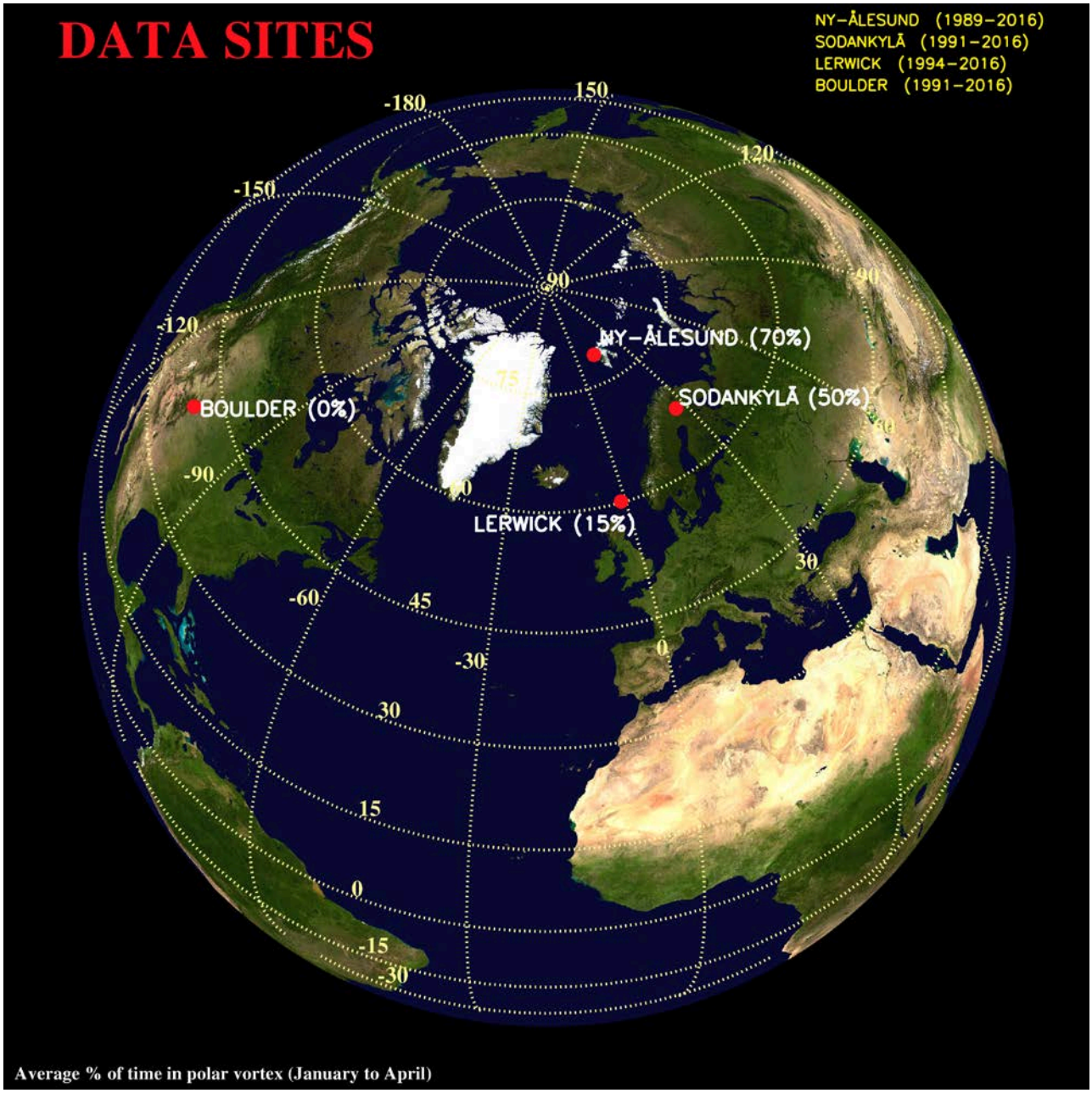

Figure 2. *Location of ground stations in the northern hemisphere used in the analyses (Figure created with IDL).*

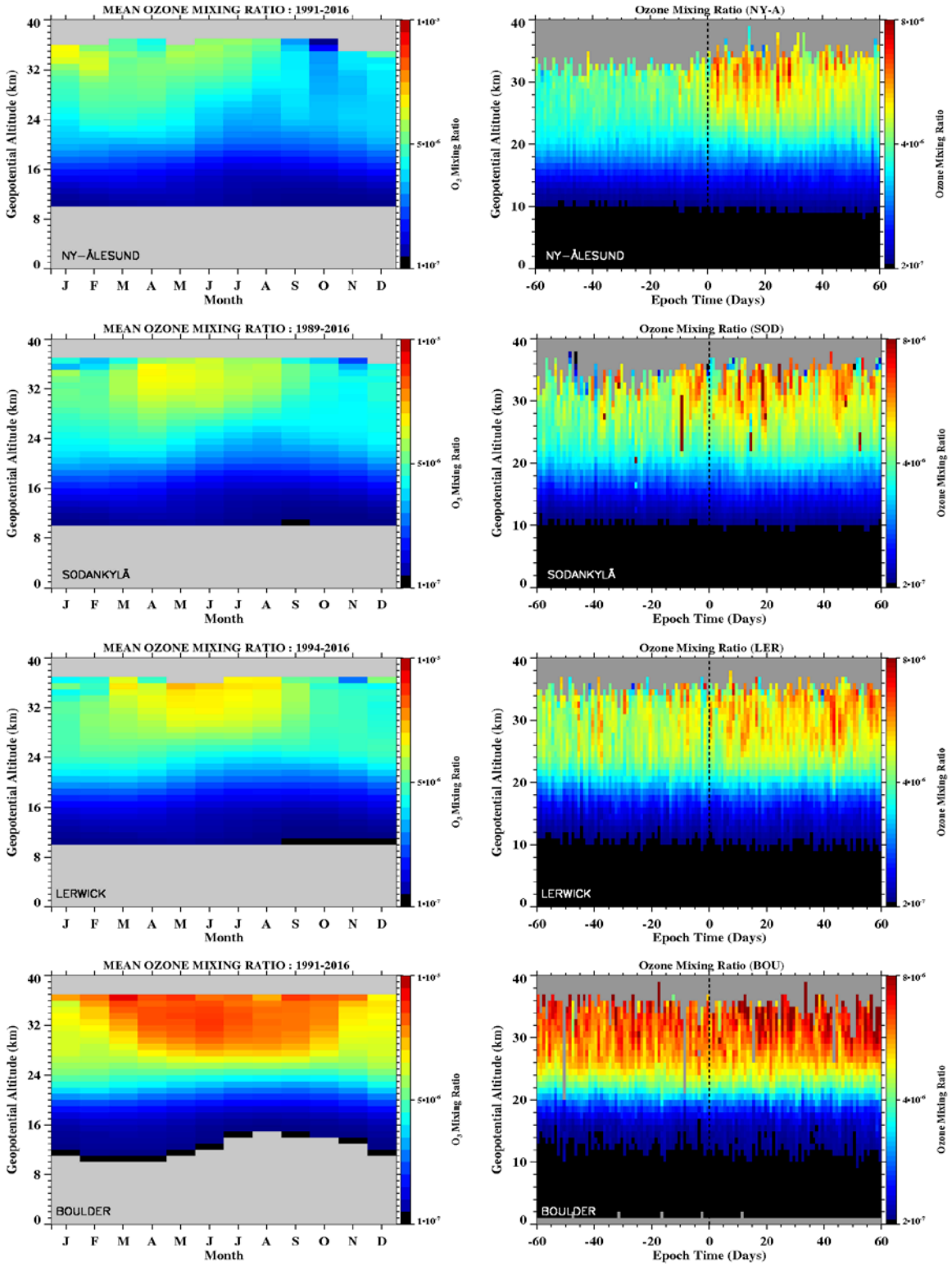

Figure 3. *Showing the mean ozone mixing ratio as a function of altitude (left column) for four sites in the northern hemisphere. Also showing the superposed change in mixing ratio at each site (right column) for the 37 SSWs. Data at the three northern-most sites (NY-ÅL, SOD, LER)) show an increase in ozone commencing with the start of the SSW events. Data from the most southerly site (BOU) show little evidence of a clear trend.*

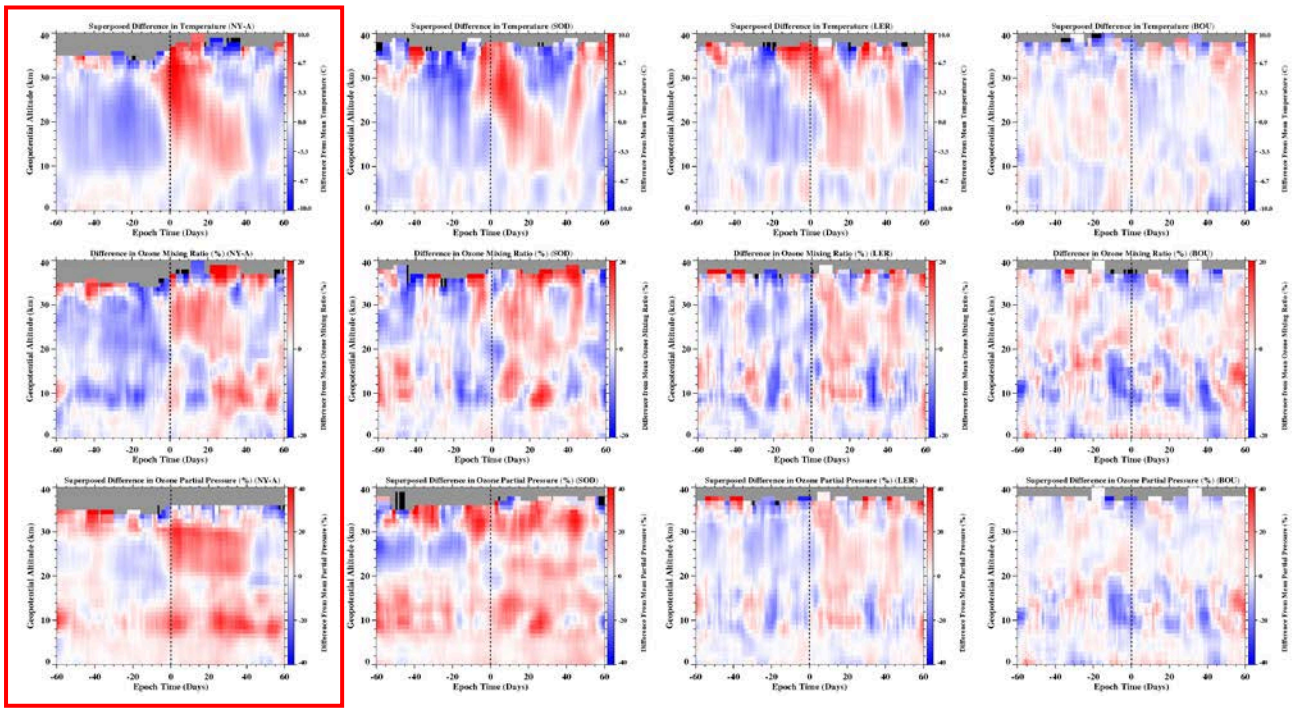

Figure 4. *Showing the superposed difference-from-mean (i.e. seasonally adjusted) ozonesonde data, superposed for the 37 SSWs. Superpositions of changes in the temperature (top row), O_3 mixing ratio (middle row) and O_3 partial pressure (bottom row) are plotted at each site. Data at the three northern-most sites (NY-ÅL, SOD, LER)) show some evidence for an increase in O_3 at the onset of the SSWs with a corresponding increase in O_3 mixing ratio and partial pressure also evident. The clearest changes are observed at NY-ÅL (red box) Data from the most southerly site (BOU) show no evidence of a clear trend in temperature or O_3.*

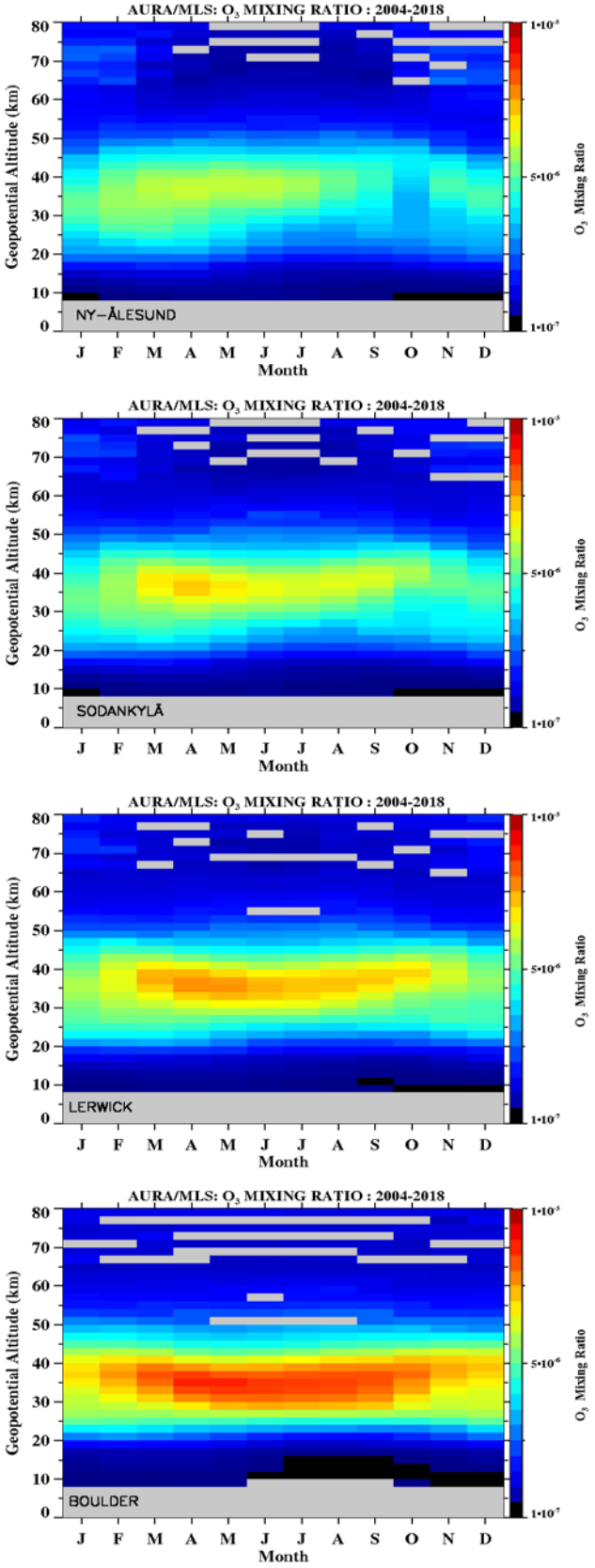

Figure 5. *Showing the mean O_3 mixing ratio measured by Aura/MLS for the four sites as a function of altitude and month.*

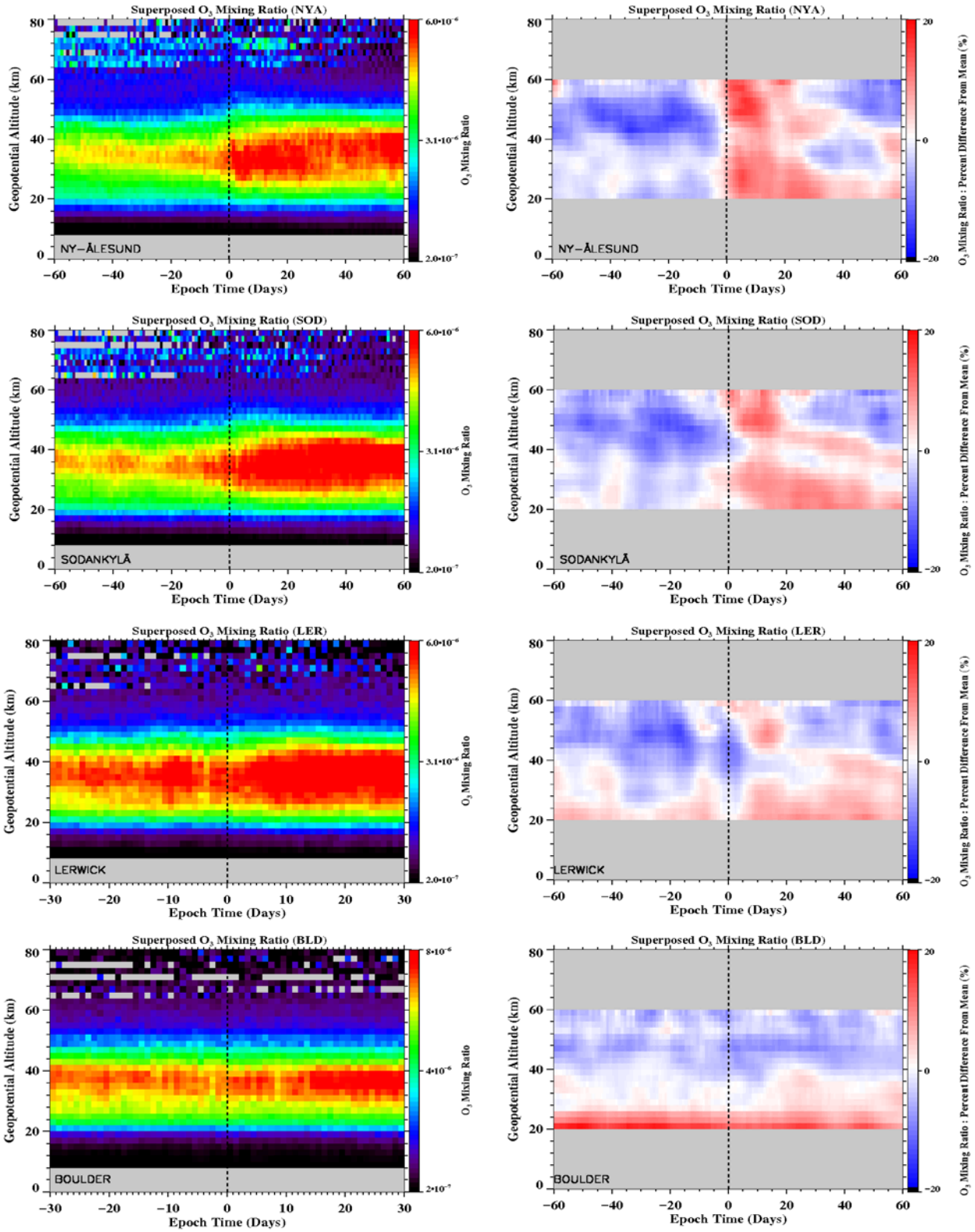

Figure 6. *Showing the superposed O_3 mixing ratio measured by Aura/MLS at the four sites for 15 SSW events. The left column is the data without any seasonal correction and the right column is the change from the mean value (seasonally-corrected). The clearest changes are evident for the highest latitude sites where the O_3 mixing ratio increases substantially at the onset of SSWs.*

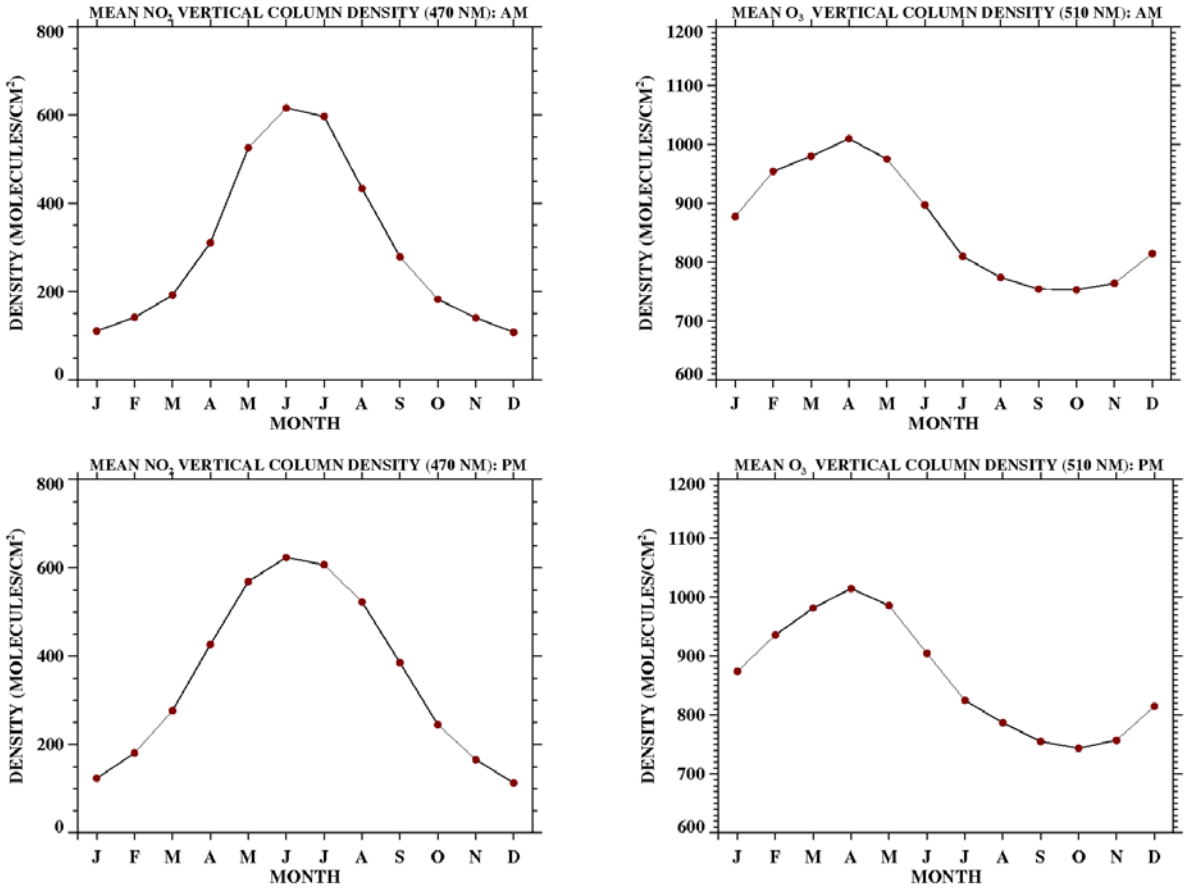

Figure 7. *Showing vertical column density of NO_2 (left) and O_3 (right) above Sodankylä as measured by the SAOZ UV-visible spectrometer during morning (top) and evening (bottom) observations. There are large annual variations in each parameter.*

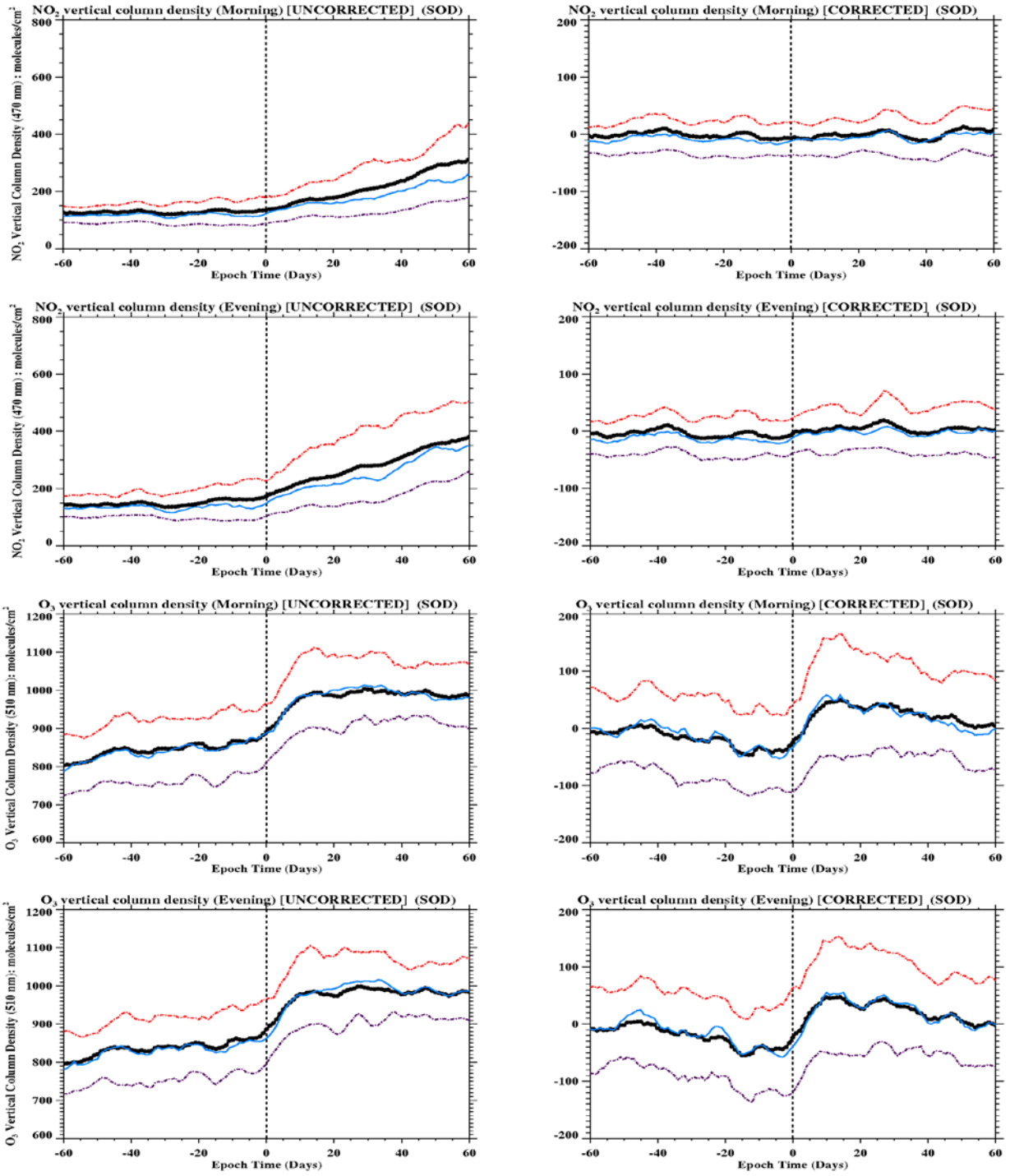

Figure 8. *Showing the superposed vertical column density of NO_2 and O_3 above Sodankylä during 36 SSWs occurring after 1989. The thick black line is the mean of the superposition while the red, blue and purple lines denote the upper quartile, median, and lower quartile of the averages. The left column shows each superposed parameter with no seasonal correction. The right column shows each superposed parameter as a difference-from-mean value. The seasonal corrections applied here demonstrate that NO_2 is little changed by the arrival of SSWs. In contrast O_3 appears to decrease slightly prior to the SSWs and then increases substantially following the SSW onset.*

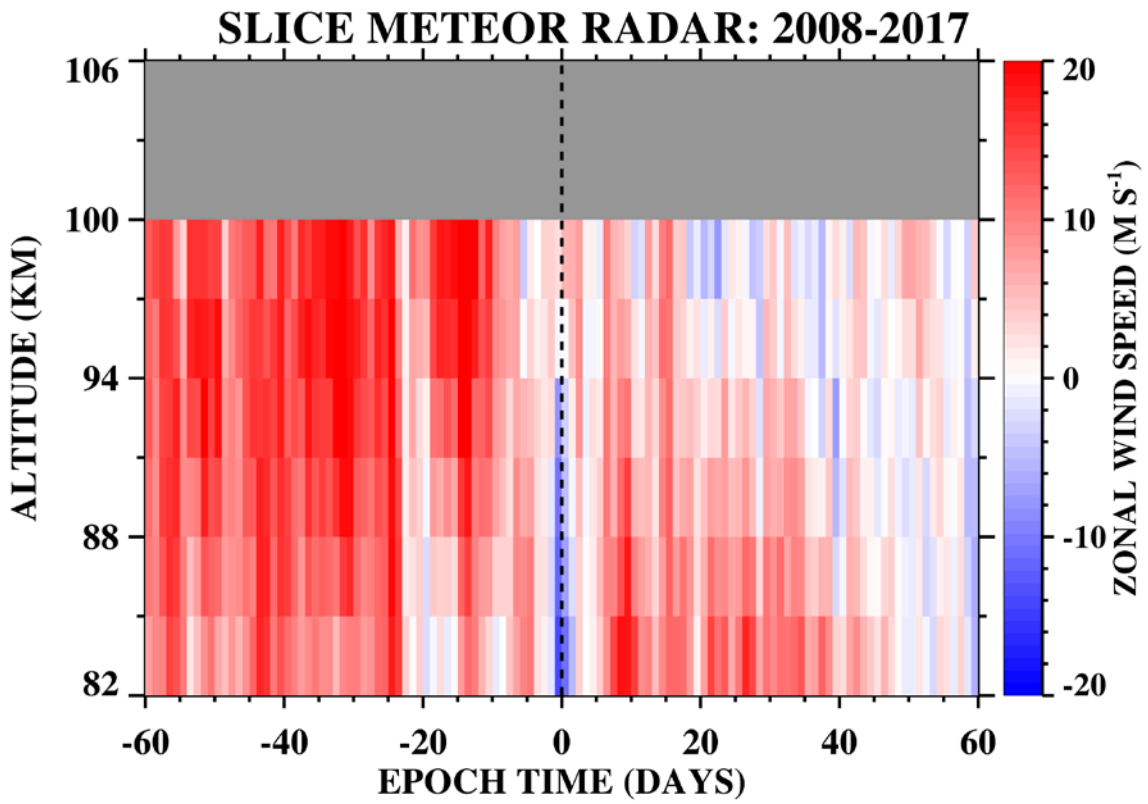

Figure 9. *Showing the zonal wind speed (west-to-east) measured above Sodankylä by the SLICE meteor radar as a function of epoch time and altitude for 9 SSWs that occur after 2008. There is a sharp reversal in wind direction at the onset of the SSWs.*

References

de la Cámara, A., J. R. Albers, T. Birner, R. R. Garcia, P. Hitchcock, D. E. Kinnison, and A. K. Smith, J. Atmos. Sci, 74, 2857-2877, 2017.

de la Cámara, A., M. Abalos, P. Hitchcock, N. Calvo, and R. R. Garcia, Response of Arctic ozone to sudden stratospheric warmings, Atmos. Chem. Phys, 18, 16499-16513, 2018a.

de la Cámara, A., M. Abalos, and P. Hitchcock, Changes in stratospheric transport and mixing during sudden stratospheric warmings, J. Geophys. Res. Atmos, 123, 3356-3373, 2018b.

Ageyeva, V.Y., A. N. Gruzdev, A. S., Elokhov, I.I. Mokhov, and N.E. Zueva, Sudden stratospheric warmings: statistical characteristics and influence on NO_2 and O_3 total contents, Izv. Atmos. Ocean. Phys. (2017) 53: 477, 2017.

Blum, L., X. Li, and M. H. Denton, Rapid MeV electron precipitation as observed by SAMPEX/HILT during high speed stream driven storms, J. Geophys. Res., 120, 3783–3794, doi:10.1002/2014JA020633, 2015.

Boyd, I., A. Parrish, L. Froidevaux, T. von Clarmann, E. Kyrölä, J. Russell, and J. Zawodny, Ground-based microwave ozone radiometer measurements compared with Aura-MLS v2.2 and other instruments at two Network for Detection of Atmospheric Composition Change sites, J. Geophys. Res. 112, D24, doi:10.1029/2007jd008720, 2007

Brasseur, G., and S. Solomon, Aeronomy of the Middle Atmosphere, 2nd ed., D. Reidel, Norwell, Mass., 1986.

Brewer, A. W. Evidence for a world circulation provided by the measurements of helium and water vapour distribution in the stratosphere, Q. J. R. Meteorol. Soc., 75, 351-363, 1949.

Butchart, N., The Brewer-Dobson circulation, Rev. Geophys., 52, doi:10.1002/2013RG000448, 2014.

Butler, A. H., D. J. Seidel, S. C. Hardiman, N. Butchart, T. Birner, and A. Match, Defining sudden stratospheric warmings, B. Am. Meteorol. Soc., 96, No. 11, 1913-1928, 2015.

Butler, A. H., J. P. Sjoberg, D. J. Seidel, and K. H. Rosenlof, A sudden stratospheric warming compendium, Earth Syst. Sci. Data, 9, 63-76, 2017.

Chau, J. L., L. P. Goncharenko, B. G. Fejer, and H-L Liu, Equatorial and Low Latitude Ionospheric Effects During Sudden Stratospheric Warming Events, Space Sci. Rev., 168, 385-417, 2012.

Damiani, A., B. Funke, M. López Puertas, A. Gardini, T. von Clarmann, M. L. Santee, L. Froidevaux, and R. R. Cordero, Changes in the composition of the northern polar upper stratosphere in February 2009 after a sudden stratospheric warming, J. Geophys. Res. Atmos., 119, 11,429–11,444, 2014.

Denton, M. H., R. Kivi, T. Ulich, M. A. Clilverd, C. J. Rodger, and P. von der Gathen Northern hemisphere stratospheric ozone depletion caused by solar proton events: The role of the polar vortex, Geophys. Rev. Lett., 45, doi:10.1002/2017GL075966, 2018.

Denton. M. H., R. Kivi, T. Ulich, C. J. Rodger, M. A. Clilverd, R. B. Horne, and A. J. Kavanagh, Solar proton events and stratospheric ozone depletion over northern Finland, J. Atmos. Sol-Terr. Phys, 10.1016/j.jastp.2017.07.00, 2017.

Denton, M. H., and J. E. Borovsky, Magnetosphere response to high-speed solar-wind streams: A comparison of weak and strong driving and the importance of extended periods of fast solar wind, J. Geophys. Res., 117, A00L05, doi:10.1029/2011JA017124, 2012.

Deshler, T., Stübi, R., Schmidlin, F. J., Mercer, J. L., Smit, H. G. J., Johnson, B. J., Kivi, R., and Nardi, B.: Methods to homogenize electrochemical concentration cell (ECC) ozonesonde measurements across changes in sensing solution concentration or ozonesonde manufacturer, Atmos. Meas. Tech., 10, 2021-2043, https://doi.org/10.5194/amt-10-2021-2017, 2017

Deshler, T., J. L. Mercer, H. G. J. Smit, R. Stubi, G. Levrat, B. J. Johnson, S. J. Oltmans, R. Kivi, A. M. Thomson, J. Witte, J. Davies, F. J. Schmidlin, G. Brothers, and T. Sasaki, Atmospheric comparison of electrochemical cell ozonesondes from different manufacturers, and with different cathode solution strengths: The Balloon Experiment on Standards for Ozonesondes, J. Geophys. Res., 113, D04307, doi:10.1029/2007JD008975, 2008.

Dobson, G., Origin and distribution of the polyatomic molecules in the atmosphere. Proceedings of the Royal Society of London. Series A, Mathematical and Physical Sciences, 236(1205), 187–193, 1956.

Dobson, G. M., Harrison, D., & Lawrence, J., Measurements of the amount of ozone in the Earth's atmosphere and its relation to other geophysical conditions. Part III. Proceedings of the Royal Society of London. Series A, Containing Papers of a Mathematical and Physical Character, 122(790), 456–486, 1929.

Dütsch, H. U., and W. Braun, Daily ozone soundings during the winter months including a sudden stratospheric warming, Geophys. Res. Lett.,7, 10, 785-788, 1980.

Ehrmann, T. S., Identification and Classification of Stratospheric Sudden Warming Events, Embry-Riddle Aeronautical University, Dissertations and Theses. 62, 2012.

Hocking, W.K., Fuller, B., Vandepeer, B., Real-time determination of meteor-related parameters utilizing modern digital technology. J. Atmos. Sol. Terr. Phys. 63, 155–169, 2001.

Jackson, D.R., and Y.J. Orsolini, Estimation of Arctic ozone loss in winter 2004/05 based on assimilation of EOS MLS observations, Q. J. Roy. Meteorol. Soc. 134, 1833-1841, doi:10.1002/qj.316, 2008.

Jiang, Y. B., L. Froidevaux, A. Lambert, N. J. Livesey, W. G. Read, J. W. Waters, B. Bojkov, T. Leblanc, I. S. McDermid, S. Godin-Beekmann, M. J. Filipiak, R. S. Harwood, R. A. Fuller, W. H. Daffer, B. J. Drouin, R. E. Cofield, D. T. Cuddy, R. F. Jarnot, B. W. Knosp, V. S. Perun, M. J. Schwartz, W. V. Snyder, P. C. Stek, R. P. Thurstans, P. A. Wagner, M. Allaart, S. B. Andersen, G. Bodeker, B. Calpini, H. Claude, G. Coetzee, J. Davies, H. De Backer, H. Dier, M. Fujiwara, B. Johnson, H. Kelder, N. P. Leme, G. Koenig-Langlo, E. Kyro, G. Laneve, L. S. Fook, J. Merrill, G. Morris, M. Newchurch, S. Oltmans, M. C. Parrondos, F. Posny, F. Schmidlin, P. Skrivankova, R. Stubi, D. Tarasick, A. Thompson, V. Thouret, P. Viatte, H.

701 Vomel, P. von Der Gathen, M. Yela, and G. Zablocki. Validation of the Aura Microwave Limb
702 Sounder ozone by ozonesonde and lidar measurements. J. Geophys. Res., 112:D24S34, 2007.
703 doi: 10.1029/2007JD008776.
704
705 Johnson, B. J., H. Vomel, S. J. Oltmans, H. G. J. Smit, T. Deshler and C. Kroger, Electrochemical
706 concentration cell (ECC) ozonesonde pump efficiency measurements and tests on the
707 sensitivity to ozone of buffered and unbuffered ECC sensor cathode solutions, J. Geophys.
708 REs., 107, D19, 4393, doi:10.1029/2001JD000557, 2002.
709
710 Kavanagh, A. J., F. Honary, E. F. Donovan, T. Ulich, and M. H. Denton, Key features of >30 keV
711 electron precipitation during high speed solar wind streams: A superposed epoch analysis, J.
712 Geophys., Res., 117, A00L09, doi:10.1029/2011JA017320, 2012.
713
714 Kivi, R., E. Kyrö, T. Turunen, N. R. P. Harris, P. von der Gathen, M. Rex, S. B. Anderson, and I.
715 Wohltmann, Ozonesonde observations in the Arctic during 1989-2003: Ozone variability and
716 trends in the lower stratosphere and free troposphere, J. Geophys. Res., 112, D08306,
717 doi:10.1029/2006JD007271, 2007.
718
719 Kishore, P., I. Velicogna, M. V. Ratnam, G. Basha, T. B. M. J. Ourda, S. P. Namboothiri, J. H.
720 Jiang, T. C. Sutterley, G. N. Madhavi, and S. V. B. Rao, Sudden stratospheric warmings
721 observed in the last decade by satellite measurements, Remote Sensing of Environment 184,
722 263-275, 2016.
723
724 Kretschmer, M., D. Coumou, L. Agel, M. Barlow, E. Tziperman, and J. Cohen, More-persistent
725 weak stratospheric polar vortex states linked to cold extremes, B. Am. Meteorol. Soc., 99, No.
726 3, 49-60, 2018.
727
728 Kuttippurath, J., and G. Nikulin, A comparative study of the major sudden stratospheric warmings
729 in the Arctic winters 2003/2004–2009/2010, Atmos. Chem. Phys., 12, 8115–8129, 2012.
730
731 Livesey, N. J, M. J. Filipiak, L. Froidevaux, W. G. Read, A. Lambert, M. L. Santee, J. H. Jiang, J.
732 W. Waters, R. E. Cofield, D. T. Cuddy, W. H. Daffer, B. J. Drouin, R. A. Fuller, R. F. Jarnot,
733 Y. B. Jiang, B. W. Knosp, Q. B. Li, V. S. Perun, M. J. Schwartz, W. V. Snyder, P. C. Stek, R.
734 P. Thurstans, P. A. Wagner, H. C. Pumphrey, M. Avery, E. V. Browell, J.-P. Cammas, L. E.
735 Christensen, D. P. Edwards, L. K. Emmons, R.-S. Gao, H.-J. Jost, M. Loewenstein, J. D.
736 Lopez, P. Nédélec, G. B. Osterman, G. W. Sachse, and C. R. Webster. Validation of Aura
737 Microwave Limb Sounder O_3 and CO observations in the upper troposphere and lower
738 stratosphere. J. Geophys. Res., 113:D15S02, doi: 10.1029/2007JD008805, 2008.
739
740 Lukianova, R., A. Kozlovsky, S. Shalimov, T. Ulich, and M. Lester, Thermal and dynamical
741 perturbations in the winter polar mesosphere-lower thermosphere region associated with
742 sudden stratospheric warmings under conditions of low solar activity, J. Geophys. Res., 120,
743 5226-5240, 2015.
744
745 McIntyre, M. E., How well do we understand the dynamics of stratospheric warmings?, J.
746 Meteorol. Soc. Japan. Ser. II, 60, No. 1, 37-65, 1982.
747
748 Manney, G. L., Z. D. Lawrence, M. L. Santee, W. G. Read, N. J. Livesey, A. Lambert, L.
749 Froidevaux, H. C. Pumphrey, and M. J. Schwartz, A minor sudden stratospheric warming with
750 a major impact: Transport and polar processing in the 2014/2015 Arctic winter, Geophys. Res.

751 Lett., 42, 7808–7816, 2015.
752
753 Manney, G. L., M. L. Santee, L. Froidevaux, K. Hoppel, N. J. Livesey, and J. W. Waters, EOS
754 MLS observations of ozone loss in the 2004-2005 Arctic winter, Geophys. Res. Lett. 33,
755 L04802, doi:10.1029/2005GL024494, 2006.
756
757 Manney, G. L., et al., Unprecedented Arctic ozone loss in 2011, Nature, 478, 469-475, 2011.
758
759 Matsuno, T., Lagrangian motion of air parcels in the stratosphere in the presence of planetary
760 waves, Pure Appl. Geophys., 118: 189-216, 1979.
761
762 Meraner, K., and H. Schmidt, Transport of nitrogen oxides through the winter mesopause in
763 HAMMONIA, J. Geophys. Res. Atmos., 121, 2556–2570, 2016.
764
765 Newman, P. A., and E. R. Nash, Quantifying the wave driving of the stratosphere, J. Geophys.
766 Res., 105, D10, 12485-12497, 2000.
767
768 Newman, P. A., E. R. Nash, and J. E. Rosenfield, What controls the temperature of the Arctic
769 stratosphere during the spring?, J. Geophys. Res., 106(D17), 19999–20010, 2001.
770
771 Päivärinta, S.-M., A. Seppälä, M. E. Andersson, P. T. Verronen, L. Thölix, and E. Kyrölä ,
772 Observed effects of solar proton events and sudden stratospheric warmings on odd nitrogen
773 and ozone in the polar middle atmosphere, J. Geophys. Res. Atmos., 118, 6837–6848, 2013.
774
775 Palmeiro, F. M., D. Barriopedro, R. Garcia-Hérrera, and N. Calvo, Comparing sudden stratospheric
776 warming definitions in reanalysis data, J. Climate, 28, 6823-6840, 2015.
777
778 Pedatella, N. M., J. I. Chau, H. Schmidt, L. P. Goncharenko, C. Stölle, K. Hocke, V. L. Harvey, B.
779 Funke, and T. A. Siddiqui, How sudden stratospheric warming affects the whole atmosphere,
780 Eos, 99, 2018.
781
782 Perry, J. S., Long-wave energy processes in the 1963 sudden stratospheric warming, J. Atmos. Sci.,
783 24, 539-550, 1967.
784
785 Pommereau, J.-P. and F. Goutail, O_3 and NO_2 Ground-Based Measurements by Visible
786 Spectrometry during Arctic Winter and Spring 1988, Geophys. Res. Lett., 15, 891–894, 1988.
787
788 Pommereau, J.-P., Goutail, F., Lefèvre, F., Pazmino, A., Adams, C., Dorokhov, V., Eriksen, P.,
789 Kivi, R., Stebel, K., Zhao, X., and van Roozendael, M.: Why unprecedented ozone loss in the
790 Arctic in 2011? Is it related to climate change?, Atmos. Chem. Phys., 13, 5299-5308,
791 https://doi.org/10.5194/acp-13-5299-2013, 2013.
792
793 Rex, M., K. Dethloff, D. Handorf, A. Herber, R. Lehmann, R. Neuber, J. Notholt, A. Rinke, P. von
794 der Gathen, A. Weisheimer, and H. Gernandt, Arctic and Antarctic ozone layer observations:
795 chemical and dynamical aspects of variability and long-term changes in the polar stratosphere,
796 Polar Research, 19, 2, 193-203, doi: 10.1111/j.1751-8369.2000.tb00343.x, 2000.
797
798 Scherhag, R., Die explosionsartigen Stratosphärenerwärmungen des Spätwinters 1951/1952,
799 Berichte des Deutschen Wetterdienstes in der US-Zone, 6, Nr. 38, 51-63, 1952.
800

Scheiben, D., Straub, C., Hocke, K., Forkman, P., and Kämpfer, N.: Observations of middle atmospheric H_2O and O_3 during the 2010 major sudden stratospheric warming by a network of microwave radiometers, Atmos. Chem. Phys., 12, 7753–7765, 2012.

Schoeberl, M. R., Stratospheric warmings: Observations and theory, Rev. Geophys., 16(4), 521–538, 1978.

Schoeberl, M. R., and D. L. Hartmann, The Dynamics of the Stratospheric Polar Vortex and Its Relation to Springtime Ozone Depletions, Science, 251, Issue 4989, pp. 46-52, 1991.

Seppälä, A., M. A. Clilverd, C. J. Rodger, P. T. Verronen, and E. Turunen, The effects of hard-spectra solar proton events on the middle atmosphere, J. Geophys. Res., 113, A11311, doi:10.1029/2008JA013517, 2008.

Shepherd, M. G., S. R. Beagley, and V. I. Fomichev. Stratospheric warming influence on the mesosphere/lower thermosphere as seen by the extended CMAM, Ann. Geophys., 32, 589–608, 2014

Smedley, A. R. D., J. S. Rimmer, D. Moore, R. Toumi, and A. R. Webb, Total ozone and surface UV trends in the United Kingdom: 1979–2008, Int. J. Climatol. 32: 338–346, 2012.

Smit, H. G. J. and the ASOPOS panel (Assessment of Standard Operating Procedures for Ozonesondes): Quality assurance and quality control for ozonesonde measurements in GAW, World Meteorological Organization, GAW Report #201, Geneva, Switzerland, 2014. available at: http://www.wmo.int/pages/prog/arep/gaw/documents/FINAL_GAW_201_Oct_2014.pdf.

Smith-Johnsen, C., Y. Orsolini, F. Stordal, V. Limpasuvan, and K. Pérot, Nighttime mesospheric ozone enhancements during the 2002 southern hemisphere major stratospheric warming, J. Atmos. Sol-Terr. Phys., 168, 100-108, 2018.

Soloman, S., Stratospheric ozone depletion: A review of concepts and history, Rev. Geophys., 37, 275-316, 1999.

Solomonov, S. V., E. P. Kropotkina, S. B. Rozanov, N. A. Ignat'ev, and A. N. Lukin, Influence of strong sudden stratospheric warmings on ozone in the middle stratosphere according to millimetre wave observations, Geomag. Aeron., 57, 3, 361-368, 2017.

Sofieva, V. F., N. Kalakoski, P. T. Verronen, S.-M. Päivärinta, E. Kyrölä, L. Backman, and J. Tamminen, Polar-night O3, NO2 and NO3 distributions during sudden stratospheric warmings in 2003–2008 as seen by GOMOS/Envisat, Atmos. Chem. Phys., 12, 1051-1066, 2012

Strahan, S. E., A. R. Douglass, and S. D. Steenrod, Chemical and dynamical impacts of stratospheric sudden warmings on Arctic ozone variability, J. Geophys. Res., 121, 11836-11851, 2016.

Tao, M., P. Konopka, F. Ploeger, J.-U. Grooß, R. Muller, C. M. Volk, K. A. Walker, and M. Riese, Impact of the 2009 major sudden stratospheric warming on the composition of the stratosphere, Atmos. Chem. Phys., 15, 8695-8715, 2015.

Tegtmeier, S., M. Rex, I. Wohltmann, and K. Krüger, Relative importance of dynamical and

chemical contributions to Arctic wintertime ozone, Geophys. Res. Lett., 35, L17801, 2008a.

Tegtmeier, S., K. Krüger, I. Wohltmann, K. Schoellhammer, and M. Rex, Variations of the residual circulation in the Northern Hemispheric winter, J. Geophys. Res., 113, D16109, doi:10.1029/2007JD009518, 2008b.

Trenberth, K. E., Dynamic coupling of the stratosphere with the troposphere during sudden stratospheric warmings, Monthly Weather Review, 101, 4, 306-322, 1973.

Tripathi, O. P., et al., The predictability of the extratropical stratosphere on monthly time-scales and its impact on the skill of tropospheric forecasts, Q. J. R. Meteorol. Soc., 141, 987-1003, 2015.

Vandaele, A. C., Fayt, C., Hendrick, F., Hermans, C., Humbled, F., Van Roozendael, M., Gil, M., Navarro, M., Puentedura, O., Yela, M., Braathen, G., Stebel, K., Tornkvist, K., Johnston, P., Kreher, K., Goutail, F., Mieville, A., Pommereau, J.-P., Khaykin, S., Richter, A., Oetjen, H., Wittrock, F., Bugarski, S., Friez, U., Pfeilsticker, K., Sinreich, R., Wagner, T., and Corlett, G., and Leigh, R.: An intercomparison campaign of ground-based UV-visible measurements of NO2, Bro, and OClO slant columns: Methods of analysis and results for NO 2 , J. Geophys. Res., 110, D08305, doi:10.1029/2004JD005423, 2005.

Vaughan, G., Roscoe, H., Bartlett, L. M., O'Connor, F. M., Sarkissian, A., Van Roozendael, M., Lambert, J.-C., Simon, P., Karlsen, K., Kastad Hoiskar, A., Fish, D., Jones, R., Freshwater, R., Pommereau, J.-P., Goutail, F., Andersen, S., Drew, D., Hughes, P., Moore, D., Mellqvist, J., Hegels, E., Klupfel, T., Erle, F., Pfeilsticker, K., and Platt, U.: An intercomparison of ground-based UV-visible sensors of ozone and NO 2 , J. Geophys. Res., 102, 542–552, 1997.

Waters, J. W., W. G. Read, L. Froidevaux, R. F. Jarnot, R. E. Cofield, D. A. Flower, G. K. Lau, H. M. Pickett, M. L. Santee, D. L. Wu, M. A. Boyles, J. R. Burke, R. R. Lay, M. S. Loo, N. J. Livesey, T. A. Lungu, G. L. Manney, L. L. Nakamura, V. S. Perun, B. P. Ridenoure, Z. Shippony, P. H. Siegel, R. P. Thurstans, R. S. Harwood, H. C. Pumphrey, and M. J. Filipiak, The UARS and EOS Microwave Limb Sounder (MLS) Experiment, J. Atmos. Sci, 56, 194-218, 1999.

Yamazaki, Y., M. J. Kosch, and J. T. Emmert, Evidence for stratospheric sudden warming effects on the upper thermosphere derived from satellite orbital decay data during 1967–2013, Geophys. Res. Lett., 42, 6180–6188, 2015.